Relationship of Lipid Rafts to Transient Confinement Zones Detected by Single Particle Tracking

Christian Dietrich,* Bing Yang,* Takahiro Fujiwara,† Akihiro Kusumi,†‡ and Ken Jacobson*§

*Department Cell and Developmental Biology, University of North Carolina at Chapel Hill, North Carolina 27599 USA; †Kusumi Membrane Organizer Project, Exploratory Research for Advanced Technology Organization (ERATO), Japan Science and Technology Corporation, Nagoya 460-0012, Japan; ‡Department of Biological Science, Nagoya University, Nagoya 464-8602, Japan; and §Lineberger Comprehensive Cancer Center, University of North Carolina at Chapel Hill, North Carolina 27599 USA

ABSTRACT We examined the physical and chemical characteristics of transient confinement zones (TCZs) that are detected in single particle trajectories of molecules moving within the membrane of C3H 10T1/2 murine fibroblasts and their relationship to "rafts." We studied the lateral movement of different membrane molecules thought to partition to varying degrees into or out of the putative lipid domains known as rafts. We found that lipid analogs spend significantly less time in TCZs compared with Thy-1, a glycosylphosphatidylinositol-anchored protein, and GM1, a glycosphingolipid. For Thy-1, we found that zone abundance was markedly reduced by cholesterol extraction, suggesting that a major source of the observed temporary confinement is related to the presence of raft domains. More detailed analysis of particle trajectories reveals that zones can be revisited even tens of seconds after the original escape and that diffusion within the zones is reduced by a factor of ~2, consistent with the zone being a cholesterol-rich liquid-ordered phase. Surprisingly, transient confinement was not strongly temperature dependent. Overall, our data demonstrate that there are raft-related domains present in certain regions of the plasma membrane of C3H cells, which can persist for tens of seconds.

INTRODUCTION

The notion of lipid rafts (Simons and Ikonen, 1997, 2000) stems from the observation that a significant fraction of plasma membrane lipids are detergent resistant (Brown and Rose, 1992). The raft concept has proved useful in organizing structural and functional knowledge concerning detergent-resistant membranes (DRM) (Brown and London, 1998a,b). Rafts, defined largely by their insolubility in various detergents, are enriched in cholesterol and sphingomyelin, glycosphingolipids (GSL), GPI-anchored proteins, and a variety of signaling molecules, potentially imparting a high degree of functional significance to these microdomains. At this juncture, there are a number of outstanding issues about rafts that preclude critical acceptance of the concept. Among them is exactly what is the in vivo correlate of the biochemically isolated DRM or rafts. Various sophisticated light microscopic techniques have produced a number of estimates of raft size ranging from 0 to 700 nm in dimension (for reviews, see Jacobson and Dietrich, 1999; Anderson and Jacobson, manuscript submitted).

One of these techniques is single particle tracking (SPT), which allows the study of particle movements and therefore also the molecules attached to the particles with submicron spatial resolution on the surfaces of living cells (Kusumi and Sako, 1996; Saxton and Jacobson, 1997). Transient confinement zones (TCZ) have been detected by SPT (Simson et al., 1995, 1998; Sheets et al., 1997). These zones, ~200 to 300 nm in diameter, in which the particle is trapped for ~5 to 10 s, were shown to preferentially trap particles attached to GPI-anchored proteins and the GSL, GM1; furthermore, the abundance and size of the zones was diminished when the biosynthesis of GSLs was depressed by inhibitors (Sheets et al., 1997). These results suggested that the zones bear some relationship to rafts.

In this paper, we examine further the physical and chemical characteristics of the TCZs in relation to "rafts." We found that zone abundance was markedly reduced by cholesterol extraction, that zones could be revisited after escape, that zone abundance was surprisingly temperature independent, and that diffusion within the zones was reduced but only by a factor of ~2. This indicates that trapping is not simply due to particles encountering a much more viscous region but suggests that some type of barrier is involved. This permanent barrier could be due to a phase boundary in the lipid matrix and/or the involvement of the membrane skeleton fence (Kusumi and Sako, 1996).

MATERIALS AND METHODS

Materials

Forty-nanometer colloidal gold functionalized with antibiotin antibodies was purchased from British Biocell International (Cardiff, UK), 1,2-dioleoyl-*sn*-glycero-3-phosphoethanolamine-fluorescein (FL-DOPE) from Avanti Polar Lipids (Birmingham, AL), 1,2-dipalmitoyl-*sn*-glycero-3-phosphoethanolamine-fluorescein (FL-DPPE), and biotinylated rabbit polyclonal antifluorescein antibodies were purchased from Molecular Probes (Eugene, OR). Biotinylated monoclonal anti-Thy-1.2 rabbit was obtained from PharMingen (San Diego, Ca). Biotin-conjugated cholera toxin B subunit (biotin-CTB) and the cholesterol-sequestering agent methyl-β-cyclodextrin (MβCD) were obtained from Sigma (St. Louis, MO).

Received for publication 21 June 2001 and in final form 15 September 2001.

Address reprint requests to Dr. Ken Jacobson, University of North Carolina, Department Cell and Developmental Biology, CB#7090, 108 Taylor Hall, Chapel Hill, NC 27599-7090. Tel.: 919-966-3855; Fax: 919-966-1856; E-mail: frap@med.unc.edu.

0006-3495/02/01/274/11 $2.00

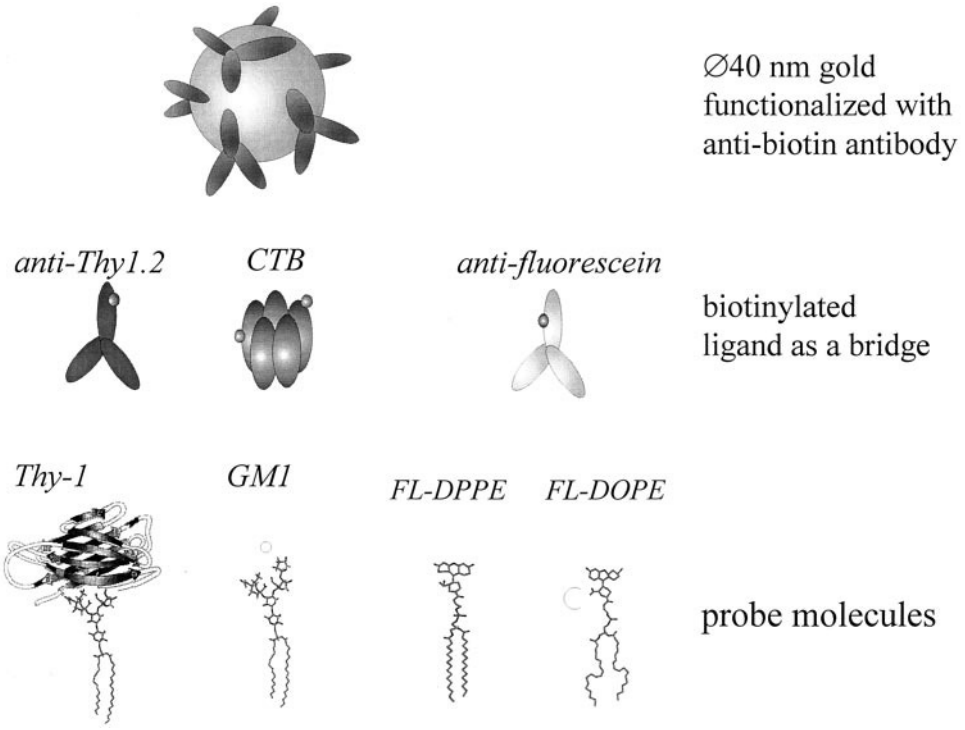

FIGURE 1 Schematic sketch illustrating the coupling scheme to bind 40 nm of colloidal gold conjugated to antibiotin antibodies to various molecules by using a biotinylated antibodies or in the case of GM1, cholera toxin B, as a bridge. Size of different components not to scale.

Cells

C3H 10T1/2 murine fibroblasts (American Type Culture Collection, Rockville, MD) were maintained in Basal Medium Eagle with Earle's salts and L-glutamine (BME) that has been supplemented with 10% fetal bovine serum, 100 units/ml penicillin, and 100 μg/ml streptomycin. Two to 4 days before an SPT experiment, fibroblasts were plated onto sterile 22 mm $\times$ 22 mm coverslips (#1.5, glass) that were placed into 35-mm petri dishes at an appropriate cell density that yielded single cells for SPT measurements.

Cells were depleted of cholesterol by treatment with 5 mM MβCD in unsupplemented BME at 37°C for 1 h. Cholesterol levels (Heider and Boyett, 1978) of C3H cells were reduced by ~60% ($\pm$10%) after a 30-min incubation with MβCD without detectable effects on cell morphology or cell activity, as judged by membrane ruffling.

Before each SPT experiment, cells on coverslips were washed three times with HAMS F12 nutrition mixture (Life Technologies/Gibco-BRL, Carlsbad, CA) supplemented with 25 mM HEPES (HH) and either mounted with spacers on a microscope slide for measurements at 22°C (room temperature) and 37°C (air curtain) or on a temperature-controlled chamber holder made from stainless steel to conduct measurements at 10 or 15°C ($\pm$1°C). Before placing the chambers on the microscope and adjusting to the desired temperature, preparation and incubation steps (see below) were conducted by injection of adequate amounts of reaction solutions into the chambers, each holding ~100 μl of solution. After the final preparation step, chambers were sealed with wax and mounted on the microscope for imaging.

Gold conjugation to cells

Gold was bound to Thy-1.2, a GPI-anchored protein, GM1, a GSL, and the two fluorescent phospholipid analogs, FL-DPPE and FL-DOPE. C3H cells expressed significant amounts of GM1, whereas a detectable level of Thy-1.2 expression occurred only in ~20% of the cells in a preparation, as judged by staining with fluorescein-CTB and anti-Thy-1.2 immunofluorescence, respectively. Synthetic phospholipid analogs were introduced in the cell membranes as follows. Fifteen microliters of 1 mg/ml lipid analog in 50:50 ethanol/chloroform (v/v) solution was placed in a borosilicate disposable culture tube and exposed to a gentle stream of Argon gas until most of the solvent was evaporated and the remaining material at the bottom of the tube was of an oily consistency. Two milliliters of warm HH (~50°C) was injected into the tube while vigorously vortexing. The pellet should dissolve completely without forming flakes. The stock solution was kept for up to 3 days at 4°C. After being mounted in sample chambers, cells were incubated with the lipid solutions at room temperature for 30 to 40 s and were then flushed with 600 μl of HH to remove unbound lipids. Fluorescence imaging revealed a uniform membrane stain, and spot fluorescence recovery after photobleaching (FRAP) measurements gave lateral mobility ($D_{\text{FL-DOPE}} = 0.33\ \mu\text{m}^2/\text{s}$; $D_{\text{FL-DPPE}} = 0.41\ \mu\text{m}^2/\text{s}$ at 37°C) and fractional recovery values ($f_{\text{FL-DOPE}} = 0.95 \pm 4\%$ and $f_{\text{FL-DPPE}} = 0.92 \pm 3\%$ at 37°C), indicating correct reconstitution of the two lipid analogs into the plasma membrane. The phenotype of cells labeled under this protocol does not differ from that of untreated cells either in morphology or activity. Moreover, if cells are labeled with FL-DOPE and trajectories for GM1 measured, they do not differ significantly from GM1 trajectories measured when no FL-DOPE is added.

We used biotinylated Thy-1.2, biotin-CTB, and biotinylated antifluorescein to bind colloidal antibiotin gold to Thy-1.2, GM1, and fluorescent lipid analogs, respectively (Fig. 1). Gold was dissolved in HAMS F12 nutrition mixture (Life Technologies/Gibco-BRL) supplemented with 25 mM HEPES and 15% serum (HHS), sedimented by centrifugation for 15 min at 11,000 $\times$ g at 4°C and redissolved in HHS. Cells mounted in the chamber were incubated for 5 min at room temperature with 100-μl-injected biotinylated ligands, which were dissolved in HH to a concentration of 10 μg/ml, and the cells were then washed with 600 μl of HH. The

gold concentration of the injection solution was adjusted to yield ~1.5 μg/ml biotin antibody bound to gold as determined from the manufacturer's specification for that lot number. We avoided a final washing step to remove unbound gold, and the sample chamber was immediately sealed with wax and mounted on the microscope; particle trajectories were recorded for the following 60 min. Even after 30 min, significant amounts of gold in the bulk did not bind to the cell, whereas the number of particles at the cell lamella (5–15 per 30 × 22-μm field of observation) remained constant. In control experiments, where cells were not incubated with biotinylated ligands, gold showed little binding to the plasma membrane (<1 gold particles per field of view), which demonstrated the specificity of the binding. Thus, specific cell surface binding appears quite stable over tens of minutes with little exchange with gold in the bulk solution.

Gold conjugation to planar model membranes

Glass supported POPC lipid bilayers were formed by vesicle fusion as described previously (Lee et al., 1991). To conjugate antibiotin gold to the lipid bilayer, we added small amounts of FL-DPPE to the lipid sample (~1 mol %), and used biotinylated antifluorescein antibody as a bridging reagent as described in the section for gold conjugation to cells. Instead of cell medium, the preparations for model system were conducted with 25 mM Hepes buffer at pH 7.3.

Time lapse gold imaging for SPT

Computer-enhanced video microscopy, described earlier (Lee et al., 1991), was used to image colloidal gold bound to different ligands in the plasma membrane of C3H cells. Briefly, the cell lamella with bound gold was imaged in brightfield mode and recorded with a video camera (Newvicon Hamamatsu). After online background subtraction and contrast enhancement with an image processing unit (Argus 20, Hamamatsu, Japan), video frames were recorded in time lapse mode (500 frames with 5 frames/s) on the hard disk of a computer (O2, Silicon Graphics, Mountain View, CA). Recorded movies were analyzed by the commercial software package ISEE (Inovision Corp., Durham, NC) that identifies relative changes of gold particle positions on the cell lamella with a precision of ±20 nm (this figure is not a standard deviation but rather characterizes the complete distribution of positional fluctuations that are measured for an immobile particle). All trajectories were visually inspected to ensure correct tracking of gold particles. Erroneous or false particle trajectories were excluded from analysis.

High-speed SPT

For image recordings with temporal resolution of 2 ms, instrumentation described elsewhere was used (Tomishige, 1998). Briefly, a digital high-speed video camera with a C-MOS sensor (model FASTCAM-Ultima; Photron, Tokyo, Japan) was used to acquire, digitize, and store images at a rate of 500 frames/s for up to 10 s. Digitized images were continuously transferred to a standard video out port, which allowed recording of video sequences on tape at the standard video rate (30 frames/sec). This camera allowed simultaneous monitoring at the video rate, and thus fast recordings could be started at any arbitrary moment during the video recording as defined by the microscopist.

Computer simulation

Particle trajectories were generated with a custom written program designed to study the effect of detection uncertainties when diffusion occurs within confinement zones. Random walks were generated by a Monte Carlo technique calculating particle jumps with random jump angle (random number generator was used from commercial programming environment; LabWindows, National Instruments, Austin, TX) and fixed jump length $l = \sqrt{4 \times D \times dt_b}$, in which D is the diffusion coefficient and dt_b, the time interval of a basic simulation step. After 100 consecutive simulation steps, the newly generated position was recorded resulting in particle trajectories with $dt = 100 \times dt_b$ time resolution.

To simulate a confinement in two dimensions, we assumed that particles were entrapped in circular domains of radius r_c. The diffusion coefficient within the domain D_{in} was assumed to be constant and was selected to be roughly consistent with experiments; however, the transfer out of the domain into the surrounding domain was restricted. For every basic simulation step that led a particle across the domain rim, an evenly distributed random number between 0 and 1 was generated and compared with a predefined escape probability levels (P_{escape}) from the interval 0 to 1. In case the generated random number fell below the critical probability level, the particle path was recalculated, assuming an inelastic reflection at the domain border, which conserved the overall jump length. Otherwise, the simulated position was accepted and used as the starting point for the next simulation step. To simulate an infinitely high barrier, P_{escape} was set to 1, which ensured entrapment of the particle in the domain.

Detection uncertainties in an experiment were caused by measurement errors and blurring effects of the recording cameras. To account for this detection noise, we displaced every trajectory point (x_i,y_i) of a simulated trajectory by a random distance (dx_i, dy_i), which was generated by assuming noise after a Gaussian distribution, characterized by the standard deviation σ_x and σ_y in the x and y directions, respectively. When not otherwise stated, simulations with noise were conducted with setting $\sigma_x = \sigma_y = 10$ nm, a characteristic value for the instrumentation used as assessed from particle trajectories from immobile gold particles.

Analysis of trajectories

In experiments with cells, we selected gold particles that moved long distances over the lamella. Immobile gold, which comprised up to 20% of the bound gold found on the cell lamella, was visually rejected in the measurement. To implement an objective criteria for long distance lateral mobility we calculated the parameter *MSD*90 (Kusumi et al., 1993), which assesses the long distance displacement (as measured for *MSD*) on basis of analyzed short-term particle mobility D_{13} (see below). We rejected trajectories with *MSD*90 < 0.3 to exclude strongly confined and stationary trajectories and trajectories with *MSD*90 > 1.9 to avoid trajectories dominated by directed motion. Note that the procedure of trajectory selection was applied to screen simulated and experimental data and affected only a small fraction (~15% for experimental and ~7% for simulated trajectories) of the data. For experimental or computer-generated particle trajectories, the mean squared displacement $MSD_{dt} = \langle \Delta x_{dt}^2 \rangle + \langle \Delta y_{dt}^2 \rangle$ of particle positions (x, y) was calculated for different time intervals dt. According to $MSD = 4 \times D \times dt$ for a randomly diffusing particle in two dimensions, we obtained D by fitting the *MSD*s at 1dt, 2dt, and 3dt to a straight line, in which dt is the basic time interval in a recording. Detection noise adds a constant offset to the *MSD*, and therefore it is not advisable to include the origin ($MSD = 0$, $dt = 0$) into the line fit (see Appendix).

Transient confinement

TCZs occurring within long-term trajectories (100 s, 5 frames/s) were detected by an algorithm described previously and characterized with respect to size and dwell time (Simson et al., 1995). To obtain a measure for the tendency of a molecule to reside in TCZs, we introduced the parameter-termed relative transient confinement time (RCT), which is defined as the ratio of detected transient confinement duration to the total recording time of the trajectories analyzed. In a few cases (~2%), the algorithm did not properly distinguish between spatial separated TCZs that were obvious upon visual inspection of the particle trajectory. These confinement zones were detected as one and therefore resulted in an

unreasonably large domain radius; such zones were excluded from analysis.

The uncertainty in RCT was computed as a standard error of the mean. This presumes that the recorded trajectories randomly sample the cell surface in an ergodic fashion, and the RCT is a measure of the partition coefficient if confinement areas are referenced to unrestricted diffusion areas. Thus, by averaging the amount of time spent in TCZs for each trajectory, we will arrive at an estimate of the degree of transient confinement that would tend to be a true mean as more and more trajectories are collected.

Revisting TCZs

The distance between two successive detected TCZs was defined as the distance between their centers of mass calculated from their associated particle positions. By definition, a particle revisited the same TCZ when the distance between the two visited TCZs was smaller than the average of the radii attributed to the TCZs (for definition of the zone radius see Simson et al. (1995)). To characterize the time between visits to successive TCZs we used the time that had elapsed between the frame when the particle left the first zone and the frame when it entered the second zone (which could on occasion be the same TCZ [i.e., revisiting]).

High time resolution SPT

To identify TCZs in high-speed recordings (500-Hz frame rate), we applied TCZ analysis (Simson et al., 1995) on the simultaneously conducted video (30 Hz) rate recordings. This allowed us to distinguish and identify zones and periods of confined and free diffusion. The frame rate allowed the acquisition of data sets with typically several 100 particle positions while a particle resided in a TCZ. For the time sequences of transient confinement, MSD_{TCZ} versus dt plots were calculated, which typically showed a saturation behavior, while the MSD_{free} versus dt plots of the remaining portions of the trajectory were linear. Displacements in the millisecond time regime are of the order of the detection noise, and this must be accounted for (see Appendix). Therefore MSD_{free} versus dt plots were fitted to a straight line for time intervals covering frame 1 to 3, i.e., dt is 2 to 6 ms. The slope of the line provided the particle mobility D_{free} in the millisecond time domain and the intersection with ordinate equaled the MSD_{noise}-offset, which was subtracted from MSD_{TCZ} to obtain noise corrected MSD_{TCZc} versus dt plots. This correction allowed inclusion of $MSD_{TCZc(dt = 0)} = 0$ as the starting point at time $dt = 0$. The initial slope of the MSD versus dt plot, and, in consequence, the diffusion coefficient within the confinement zone, was determined as $D_{TCZ} = f \times MSD_{TCZc(dt = 2\ ms)}/(4 \times dt_{(dt = 2\ ms)})$ in which f is a correction factor determined from Monte Carlo simulations (see Appendix). We tested this procedure on simulated particle trajectories and found that this protocol reproduced the diffusion values injected into the simulation within a few percent. The domain radius r_c was obtained from the saturation level of MSD_{TCZc} in the limit of long-interval times (Appendix). The ratio D_{TCZ}/D_{free} provided a measure of the differences of the membrane mobility between the TCZ and surrounding membrane.

RESULTS

Labeling various raft components for SPT

To address the differential partitioning of several representative membrane molecules into putative lipid microdomains, SPT was applied to follow the movements of Thy-1, a GPI-anchored protein, GM1, a representative GSL, as well as fully saturated FL-DPPE and unsaturated FL-DOPE fluorescent lipid analogs on the surface of fibroblasts. As depicted in Fig. 1, 40 nm colloidal gold conjugated with antibiotin antibody was attached to these molecules using a biotinylated ligand as a bridging component. Thus, the same antibiotin conjugated gold could be used to tag the investigated molecules with similar spacing between the colloidal gold and the cell membrane.

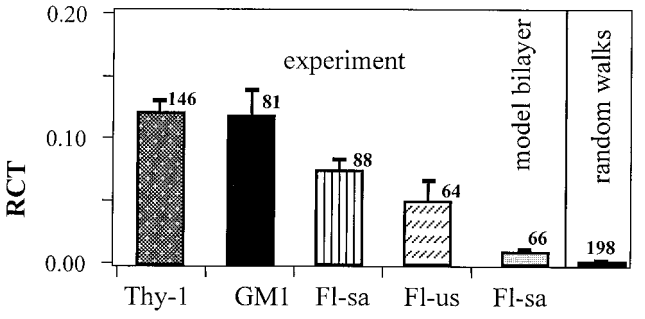

FIGURE 2 RCT analyzed from time lapse SPT recordings conducted with C3H fibroblasts at 37°C for the molecules investigated. For comparison, the RCT for FL-DPPE (1 mol %) in a planar supported POPC bilayer (at 22°C; see Material and Methods) is given. The RCT for computer simulated random walk trajectories is shown on the right panel. Numbers indicate number of trajectories analyzed for each molecule. Error bars reflect the mean ± SE (see Materials and Methods).

Relative confinement for putative raft components

We analyzed particle movement of the different membrane probes for 100-s observation times. We applied an algorithm previously described (Simson et al., 1995) to detect TCZ within the long-term trajectories. To compare the tendency of the different probe molecule to undergo transient confinement, we introduce the RCT, which is defined as the ratio of the time a particle spends in TCZs to the total recording time of the trajectory. Fig. 2 shows the average RCTs calculated from sets of particle trajectories that were recorded for the different molecules investigated. The RCT values indicate Thy-1 and GM1, both putative raft occupants, spend similar and the largest amounts of time in the TCZs. Even lipid analogs experience smaller but significant transient confinement when moving laterally in the plasma membrane of C3H fibroblasts with the fully saturated analog confined more than the unsaturated analog. By contrast, trajectories obtained from particles attached to FL-DPPE embedded in a planar supported model membrane system (see Materials and Methods) revealed negligible transient confinement (Fig. 2). As a negative control, the RCT analyzed from random walk particle trajectories generated by computer assuming lateral diffusion in a homogeneous membrane is given (right panel, Fig. 2). The negligible RCT obtained confirms that the algorithm with the parameter settings used is robust against the statistical variations inherent in Brownian diffusion.

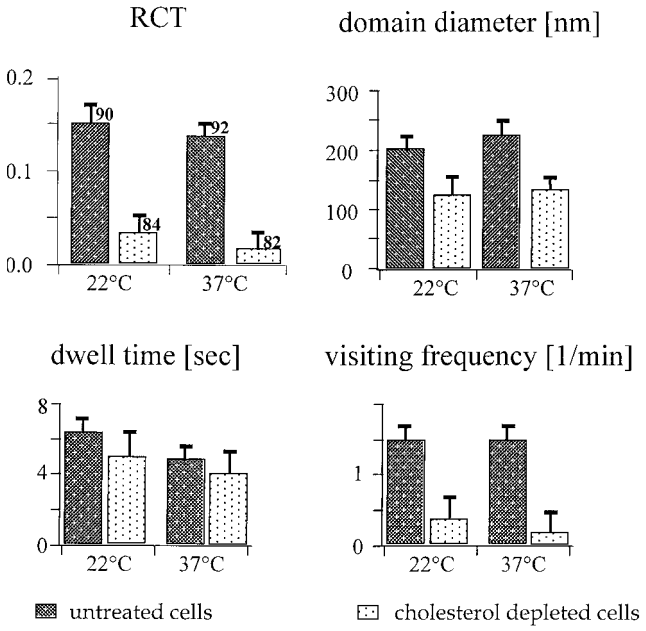

FIGURE 3 Effect of cholesterol depletion on abundance of RCT measured for Thy-1 (*top left*), the average diameter (*top right*), the average dwell time (*bottom left*), and average frequency of visits to TCZs (*bottom right*) at 22 and 37°C. Cholesterol depletion and control experiments were conducted identically except for the addition of 5 mM MβCD into the BME incubation solution (see Material and Methods). Number of analyzed trajectories are indicated in histogram bars in top right panel. Error bars reflect the mean ± SE.

Chemical and physical characteristics of TCZs

Cholesterol extraction reduces TCZ abundance

Earlier, we showed that GSL depletion by metabolic inhibition of GSL biosynthesis resulted in a considerable reduction in TCZ abundance and size (Sheets et al., 1997). We used MβCD as a cholesterol extraction reagent and found that ~60% extraction of cell cholesterol results in a major reduction in TCZ abundance at both 37 and 22°C, as inferred from the decrement in RCT (Fig. 3, top left panel). Note that in the unextracted controls, mean domain diameters are ~200 nm and dwell times are ~5 s (Fig. 3, top right and bottom left panels, respectively). A significant reduction of the size and dwell time of the remaining TCZs (Fig. 3, top right and bottom left panels, respectively) was also observed. The lower right panel shows, that as expected, the frequency of visiting TCZs drops drastically after cholesterol extraction. These findings are consistent with the hypothesis that TCZs reflect lipid rafts that are dependent on cholesterol for their integrity (Simons and Ikonen, 1997, 2000).

Diffusion within TCZs is reduced

To carefully examine diffusion of Thy-1 within TCZs, we used a high-speed camera to record bright field images every 2 ms for a period of 10 s. The high-speed recording was randomly activated while the particle position was recorded at the video rate (see Materials and Methods). The video rate (30 Hz) recording allowed application of the TCZ analysis revealing time periods and regions of temporary confinement. By chance, these events may be overlaid with the high-speed recording, as illustrated in Fig. 4 *a* (with a high magnification inset). In Fig. 4 *b*, corresponding plots depicting the displacements in *x*-direction as a function of time (Fig. 4, bottom panel) and the calculated likelihood profile (Fig. 4, top panel) are given. From such measurements, *MSD* versus time plots could be constructed from the high-time resolution trajectories both inside and outside of the TCZs (Fig. 4 *c*). Outside the TCZ, the linear *MSD* versus time plot indicates the free diffusive behavior with the diffusion coefficient, D_{out}, calculated from the slope of the line between points 1 and 3. The *MSD* plot calculated for periods, when the particle resided in the TCZ saturated quickly, indicating confined diffusion. We applied a more sophisticated analysis described in the Materials and Methods and Appendix sections to deduce D_{in} and size for the domains as compiled in Table 1. The measured values for D_{out} and D_{in} vary significantly for different particles; however, the relative reduction in diffusion, D_{in}/D_{out}, indicates a similar modest reduction of the particle mobility by a factor of ~2 (Table 1). This reduction is in line with what one would expect for a cholesterol-rich liquid ordered phase (Wu et al., 1977; Almeida et al., 1992), such as is postulated for rafts (Simons and Ikonen, 1997). This moderate reduction indicates that the observed particle confinement is not due to the particle entering a zone of much greater viscosity but rather that the particle experiences an significant activation barrier, which it has to overcome to escape from the confinement zone.

TCZs can be revisited

We also studied the temporal and spatial distribution of TCZs for Thy-1 and GM1. Interestingly, we find that particles revisit TCZs (for illustration, see particle trajectory in Fig. 5 *a*). For Thy-1 and GM1 we find that 12 and 26% of the TCZs for these components, respectively, are revisited. The distribution of times between successive visits to the same zone is depicted in the histograms in Fig. 5 *b* and indicates for Thy-1 that revisiting of the same zone can occur even up to 80 s after the first visit. This implies that at least certain zones were stable for 80 s or longer.

Interzone distances are broadly distributed

Fig. 5, *c* and *d* gives the interzone distance distribution and the distribution of times between visiting successive TCZs for GM1 and Thy-1, respectively. We were particularly interested if molecules undergoing transient confinement reflect the hop diffusion of a molecule from one zone to the

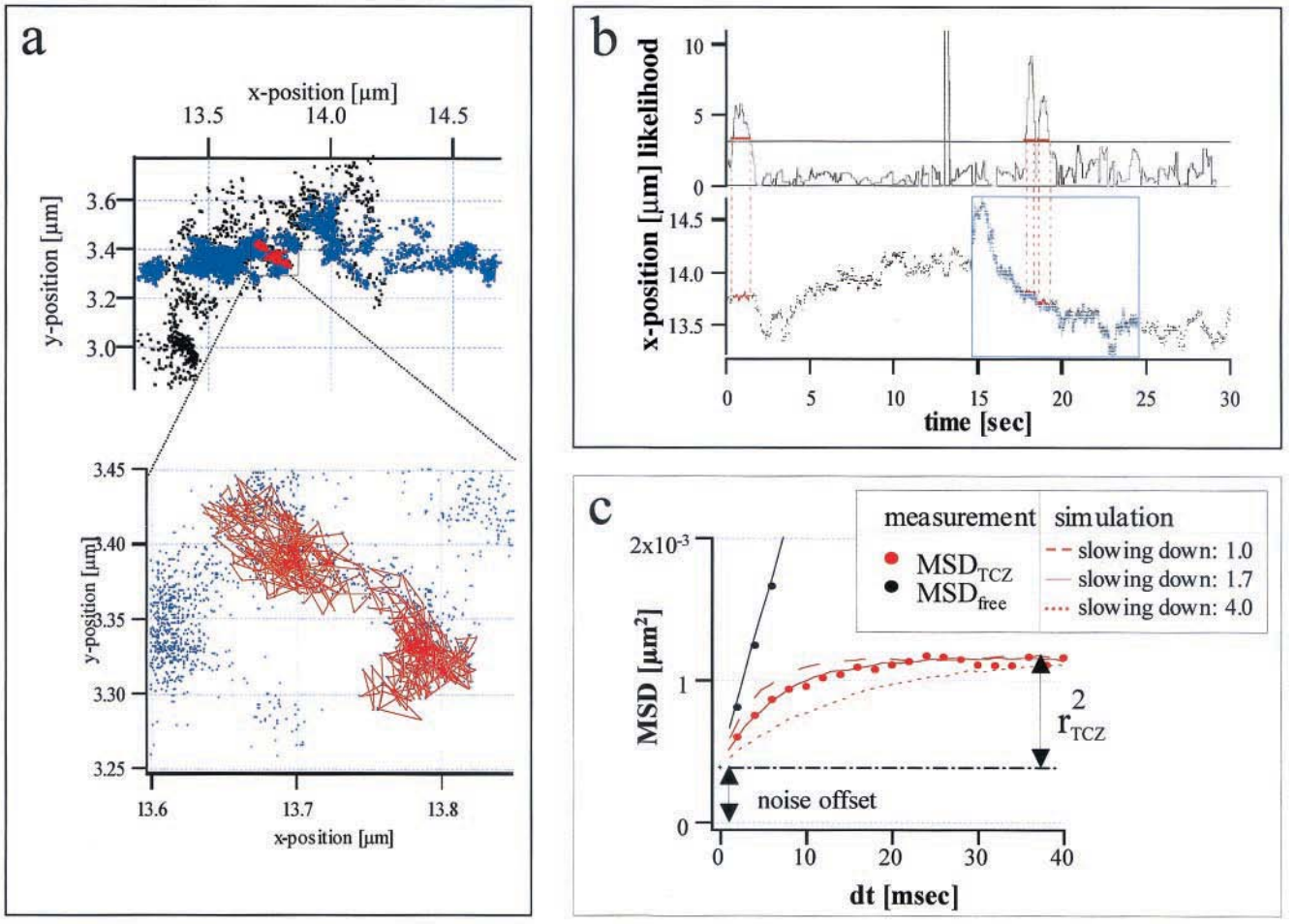

FIGURE 4 (*a*) Example of particle trajectory (*top*) obtained from analysis of a video rate recording conducted for a gold particle, which was bound to Thy-1 on the cell membrane. By chance (see Methods), confinement behavior occurred while, simultaneously, 5000 image frames were recorded into a specialized digital memory. Inset shows an identified TCZ (*red*). (*b*) Likelihood profiles (*top*) were calculated from this recording to identify trajectory segments of nonrandom particle movement. TCZs were defined as the time periods when the likelihood level surpassed a critical probability level L_c, denoted by the horizontal line above the abscissa. Note, only events that comprise at least 10 subsequent trajectory points were accepted as TCZs. Therefore, only the red segments on the L_c line were accepted as TCZs. The bottom panel gives the *x* component versus time, which levels off during transient confinement. (*c*) Identifying TCZs in the high-speed recording allows calculation of *MSD* versus *dt* plots for segments of confined and free diffusion. As described in the Appendix, we deduced the particle *D* values inside and outside of the TCZ.

adjacent confinement region. We find that a particle can travel several microns before it again encounters a TCZ. This results in a wide variation from nearest neighbor zones ($<$0.5-μm separation) to trajectories that have only one or no TCZ; in fact, these later categories are most prevalent as shown earlier for a GPI-anchored neural cell adhesion molecule isoform (Simson et al., 1998). By contrast, strict conformance to the membrane skeleton fence model would predict that a particle attached to a membrane protein most often hops to a neighboring corral (Kusumi and Sako, 1996).

Temperature dependency of TCZs

Fig. 6 shows the temperature dependence of RCT, zone diameter, and duration of confinement for GM1. Surprisingly, within the considerable uncertainty of the measurement, there was not significant temperature dependence. Similar results were obtained for Thy-1, FL-DPPE and FL-DOPE (data not shown).

DISCUSSION

In this study we find several lines of evidence that TCZs detected in particle trajectories reflect the presence of putative lipid microdomains. First, the abundance of TCZs strongly depends on the presence of cholesterol, consistent with the hypothesis that the integrity of rafts depends on appropriate levels of cholesterol (Simons and Ikonen, 1997, 2000). Second, the measured reduction of particle mobility after entering a TCZ is modest, in line with the interpreta-

TABLE 1 Mobility retardation within TCZs*

Trajectory	D_{out}	$D_{in\text{-}correct}$	$\frac{D_{out}}{D_{in\text{-}corrected}}$	Domain diameter (nm)
1	7.51	4.4	1.7	110
2	3.22	1.5	2.1	112
3		2.1	1.6	146
4	7.40	4	1.9	624
5	7.04	3.2	2.2	126
6		3.7	1.9	140
7		4	1.8	128
8		3.9	1.8	108
9	3.81	2.7	1.4	102
10		3	1.3	80
11		2.8	1.3	138
12	2.13	1	2.1	90
13	2.30	1.5	1.5	92
14		1.4	1.6	66
15		1.6	1.4	40
16		1.7	1.4	52
Mean value			1.67	134 nm

*D_{out}, D outside of the TCZ; $D_{in\text{-}corrected}$, D inside TCZ corrected as described in Appendix.
Domain diameters calculated from the estimated saturation value of *MSD* versus *dt* curves were smaller than those calculated from the conventional TCZ analysis.

tion that rafts reflect the existence of lipid domains in a liquid ordered, cholesterol-enriched phase. Third, we find that the abundance of TCZs depends on the membrane molecule investigated. Thy-1, a GPI-anchored protein was found to be significantly enriched in the DRM fractions in neurons (Madore et al., 1999) and in lymphoid cells (Hoessli and Rungger-Brandle, 1985; Draberova and Draber, 1993) and, on this basis and based on corollary electron microscopy (Madore et al., 1999), was suggested to be present in membrane rafts. The GSLs, including GM1, are also thought to partition favorably into rafts (Brown and London, 1998a,b; Stauffer and Meyer, 1997; Dietrich et al., 2001). Consistent with this, we find a significantly higher tendency for these probe molecules to reside in TCZs compared with the phospholipid analogs. The lowest value for RCT is measured for FL-DOPE, which would be thought least likely to enter rafts due to its unsaturated acyl chains, making partitioning into the more ordered raft phase unfavorable.

Current limitations

Labeling

Although we devised a scheme (Fig. 1) in which the same colloidal gold can be coupled to various target molecules via a biotinylated ligand as a bridging component, in fact, the absolute valency of the observed complexes cannot be determined. This limitation may produce a range of partitioning into various membrane domains including rafts, due to a possible light degree of cross-linking.

TCZ analysis

The algorithm to detect TCZs was optimized to pick up anomalies in the video rate trajectories in which sometimes transient confinement is obvious by inspection (Simson et al., 1995). However, hop diffusion on a very fine scale (Suzuki et al., 2001) is generally not detected. This is because the time (approximately microseconds) and distance scales (approximately tens of nanometers) needed to visualize the membrane skeleton fence in full detail require much higher temporal resolution than are needed to visualize TCZs, which are normally separated by hundreds of nanometers and in which the particle resides for ~5 s.

Models for TCZs and their relationship to lipid rafts

Several alternative models could account for the data (Jacobson and Dietrich, 1999). Of course, at this stage of development of the raft field, these models do not comprise an exhaustive list. First, zones could simply be contiguous cholesterol-dependent liquid ordered regions ~200 nm in dimension. This model would readily account for the loss of TCZs upon cholesterol extraction and the slightly slower diffusion within the TCZ. As demonstrated in model membrane systems (Dietrich et al., 2001), fluid-fluid phase coexistence can provide quite measurable differential partitioning with a high rate of molecular exchange between phases. Thus, the boundary between the liquid crystalline and the liquid-ordered phase would not, in itself, provide the duration of confinement required. An effective "barrier" would be indicated if the partition coefficients for GPI-anchored proteins and GSL were very favorable. However, with few exceptions (Schutz et al., 2000), fluorescent stains of putative raft components, in an uncross-linked state, show little unambiguous evidence of localized concentrations of such components. A cytoskeletal barrier could be provided by the membrane apposed cytoskeleton as transmembrane proteins linked to the underlying cytoskeleton would provide a "picket fence" that is able to restrict the diffusion of GPI-anchored proteins residing in the outer monolayer of the plasma membrane (Sheets et al., 1997). Cytoskeletal components including actin (Rodgers and Zavzavadjian, 2001; Holowka et al., 2000), annexin (Oliferenko et al., 1999), and filamin (Stahlhut and Deurs, 2000) have been found associated with rafts and/or caveolae. The phenomenon that zones can be revisited by the same particle implies a stable location most likely originating in membrane-cytoskeletal interactions. However, preliminary attempts to date to perturb this putative interaction with drugs have not met with success. In regard to a cytoskeletal basis for confinement, the lack of a temperature dependence is something of a conundrum. If confinement is not due to viscous trapping, why is not a significant activation energy seen for escape (dwell time) from the TCZ?

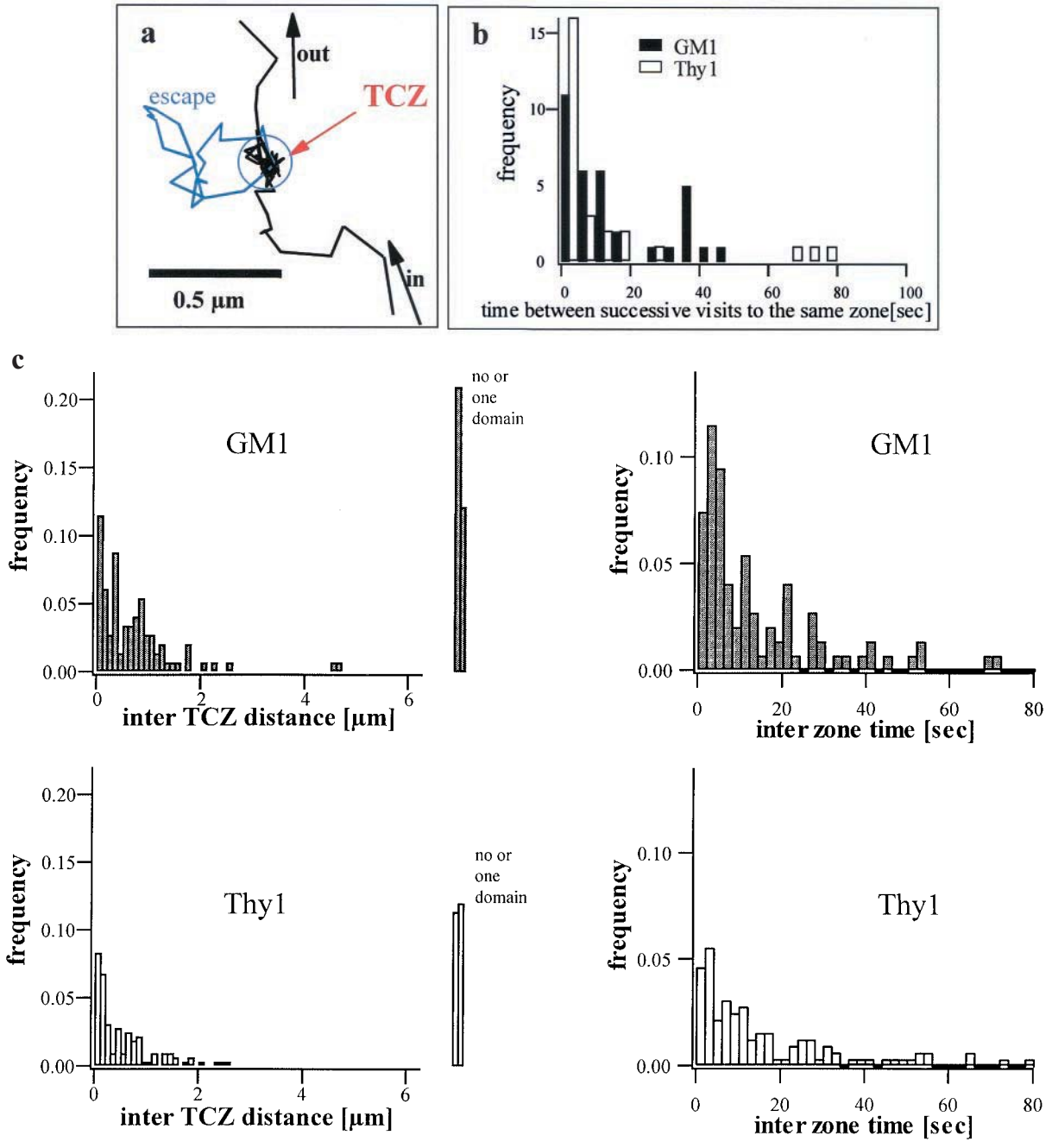

FIGURE 5 (*a*) Revisiting phenomena is illustrated in the trajectory (*left*) for a gold particle bound to GM1 (C3H cells at 37°C). Blue portion of the trajectory indicates escape and revisit. (*b*) Histogram of the distribution of time between successive visits to the same zone for GM1 (*black bars*) and Thy-1 (*open bars*). (*c*.) Inter-TCZ distance (*left panels*) and interzone time (*right panels*) between two successive TCZs contained in one trajectory for GM1 (*top*) and Thy-1 (*bottom*).

In Monte Carlo simulations that assume a domain radius independent of temperature, we found that escape probabilities in the range of $p \sim 0.2$ (this corresponds to an activation energy of 1.6 k_BT at 37°C) reproduce the weak temperature dependence of transient confinement. However, to obtain this result, diffusion had to be ~10 times slower within the TCZ compared to outside of the TCZ, whereas the measured $D_{out}/D_{in} \sim 2$. At this point, one might speculate that the model, using the measured D_{out}/D_{in}, produces erroneous results because it assumes normal (not anomalous) diffusion within the TCZs.

Alternatively, rafts could be considerably smaller than the measured zone diameters, and the entire raft might

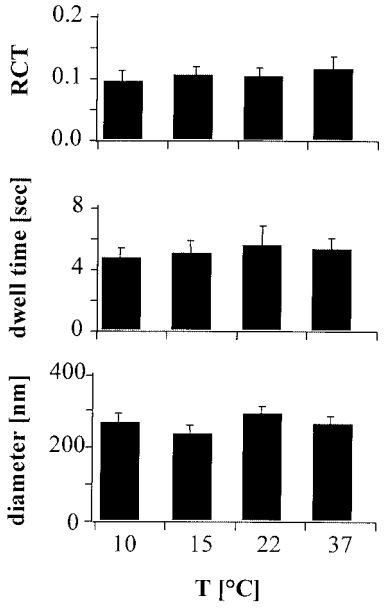

FIGURE 6 Temperature dependence of RCT (*top*), dwell time (*middle*), and zone diameter (*bottom*) measured for gold particles bound to GM1 (*black bars*). Error bars reflect the mean ± SE.

diffuse into a TCZ, become trapped for ~5s, and then escape. Such entities might be of the size suggested by Varma and Mayor (1998) and Pralle et al. (2000). Or they might be even smaller—the lipid shells postulated by R. Anderson and K. Jacobson (manuscript submitted) to surround individual GPIAPs—such that a gold particle might bind one or several shells. In this sort of model, cholesterol depletion would dismantle the elementary raft or shell and thereby prevent extensive transient confinement. Diffusion would be slower within the TCZ because of an elementary raft or shell concentration with the zone-producing obstructed diffusion.

APPENDIX

Effect of detection noise on *MSD* plots

For high-speed recordings conducted in this study, particle displacements between two time frames are of the same magnitude of the spatial detection noise. Assuming a particle with $D = 7 \times 10^{-10}$ cm^2/s, one obtains a mean jump distance of ~17 nm for a 2-ms time interval. Fig. 7 *a* shows *MSD-dt* plots calculated from simulated trajectories assuming a random walk (open squares) and random walk with superposed Gaussian distributed noise (filled circles). We generated *MSD-dt* plots from simulated trajectories assuming unrestricted diffusion (straight lines) and diffusion restricted to a circular domain (saturating curves) characterized by an infinitely deep potential well ($P_{\text{escape}} = 0$).

For an immobile particle the *MSD* is zero; however, it differs from zero if the spatial detection noise is included, which results in apparent displacements and shifts the *MSD*-plot at all time frames by a constant value MSD_{noise}. For our instrumentation, detection uncertainties of immobile particles are well described with a normal distribution probability. Then,

$$MSB_{\text{noise-gauss}} = \frac{1}{\sqrt{2\pi}\sigma_x}\int_{-\infty}^{+\infty}\exp\left(-\frac{y^2}{2\times\sigma_x{}^2}\right)dy$$

$$\times\frac{1}{\sqrt{2\pi}\sigma_y}\int_{-\infty}^{+\infty}\exp\left(-\frac{x^2}{2\times\sigma_y{}^2}\right)\times(x-y)^2dx$$

in which σ_x and σ_y are the standard deviations in x and y direction, respectively. Thus, from knowledge of the spatial noise level, one obtains the corrected MSD_c-dt plot by subtraction of MSD_{noise} for all time frames other than $dt = 0$, in which $MSD_c(dt = 0) \equiv 0$.

Extraction of D_{in} for particles entrapped in a circular domain

For a circular domain geometry, the MSD_{TCZ}-plot saturates to the value $MSD_{\text{TCZ}}(dt \to \infty) = r_c{}^2$ (Saxton and Jacobson, 1997). For short time periods, when the particle does not experience the barrier at the domain rim, the diffusion is free and the initial slope of the plot gives the diffusion coefficient of the particle within the domain with $4 \times D_{\text{in}} = d(MSD_{\text{TCZc}})/d(dt)|_{dt=0}$. It was important to inquire whether the initial slope is reasonably well represented by the slope as obtained form the first two points of a noise corrected MSD_c-dt plot. Therefore, we generated trajectories, simulating particles stably entrapped ($P_{\text{escape}} = 0$) in a circular domain for different particle mobilities and domain diameters and assuming a particle detection rate of 500 Hz. Fig. 7 *b* shows a selection of *MSD-dt* plots after correction of the noise related *MSD* shift with typical experimental parameter settings. The *MSD-dt* plots are given in dimensionless units, ($[MSD_{\text{scale}}] = [MSD/r_c^2]$; $[dt_{\text{master}}] = [dt \times D_{\text{in}}/r^2]$), resulting in the overlay of all simulated curves that obey the boundary conditions: $\partial(MSD_{\text{master}})/\partial(dt_{\text{master}})|_{dt=0} = 4$ and $MSD_{\text{master}}|_{dt\to\infty} = 1$. The first data point at $dt_{\text{master}}(1)$ in the MSD_c plot then provides an estimate for the mobility of the particle: $D_{\text{estimate}} = MSD_{\text{master}}(1)/(4 \times dt_{\text{master}}(1))$. Simulations were conducted with different temporal resolutions to obtain factors by which D measured from increasing time intervals is underestimated for typical experimental settings (inset in Fig. 7 *b*). We found that the slope of the first two time points systematically underestimated the "true" D by ~10% for parameter settings that are typical for our experiments. However, this was small compared with the mobility variation experimentally measured for different TCZs.

We thank Thierry Horner for working out the cholesterol depletion assay and Alex Valm for assistance conducting SPT measurements.

This work was supported by the National Institutes of Health (GM41402, to K.J.) and the Deutsche Forschungsgemeinschaft Scholarship (Di 691/1-1, to C.D.), and the ERATO Kusumi Membrane Organizer project (to A.K.).

REFERENCES

Almeida, P., W. Vaz, and T. Thompson. 1992. Lateral diffusion in the liquid phases of dimyristoylphosphatidylcholine/cholesterol lipid bilayers: a free volume analysis. *Biochemistry.* 31:6739–6747.

Brown, D. A., and E. London. 1998a. Functions of lipid rafts in biological membranes. *Annu. Rev. Cell Dev. Biol.* 14:111–136.

Brown, D. A., and E. London. 1998b. Structure and origin of ordered lipid domains in biological membranes. *J. Membr. Biol.* 164:103–114.

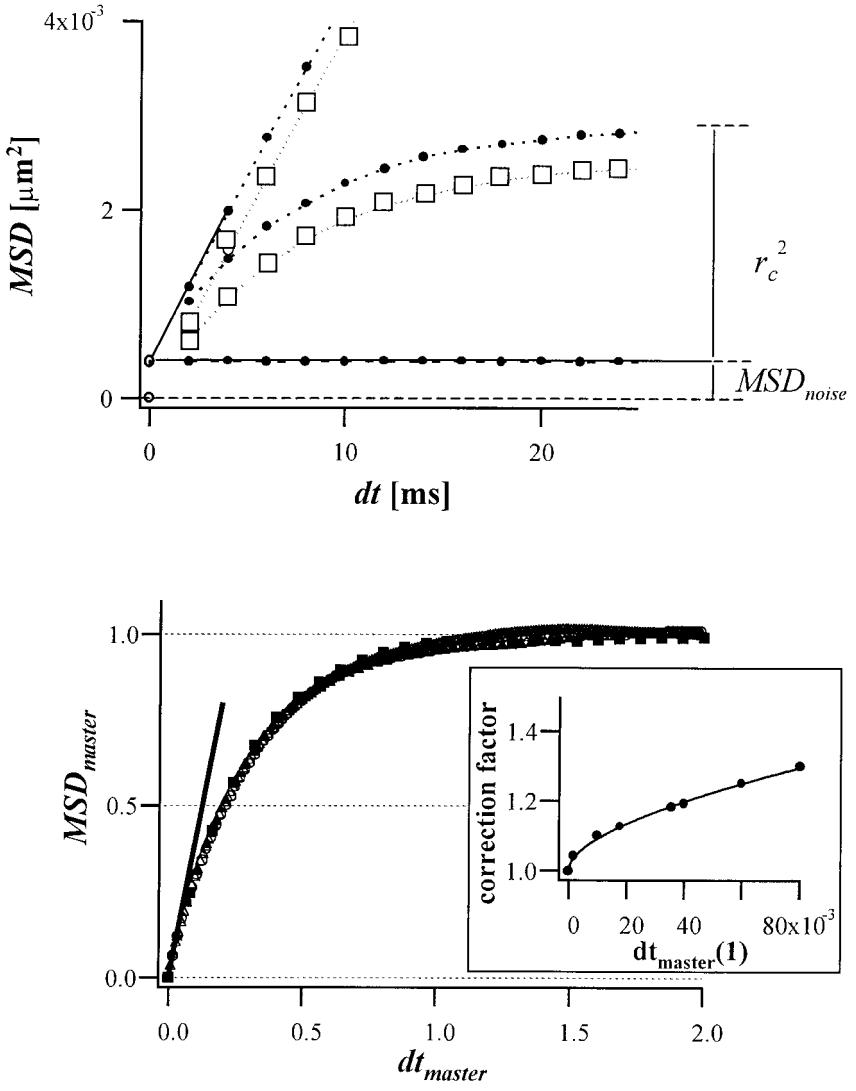

FIGURE 7 (*a*) *MSD-dt* plots were calculated from computer generated trajectories, excluding (□) or including Gaussian distributed spatial noise ($\sigma_y = \sigma_x = 10$ nm; ●). Linear *MSD-dt* plots result from simulations assuming unrestricted diffusion whereas saturation in *MSD-dt* plots occurs when particle motion is restricted to a circular domain of 50-nm radius and infinitely high barrier at the boundary ($P_{escape} = 0$). For these plots, the detection rate was 500 Hz, and the particle diffusion constant was $D_{in} = 5$ cm $\times 10^{-10}$/s. (*b*) *MSD*-plots in dimensionless units (see Appendix) obtained from simulations with different parameter settings: ($D_{in} = 10 \times 10^{-10}$ cm^2/s, r = 50 nm); ($D_{in} = 10 \times 10^{-10}$ cm^2/s, r = 75 nm); ($D_{in} = 5 \times 10^{-10}$ cm^2/s, r = 75 nm); ($D_{in} = 5 \times 10^{-10}$ cm^2/s, r = 100 nm).

Brown, D. A., and J. Rose. 1992. Sorting of GPI-anchored proteins to glycolipid enriched membrane subdomains during transport to the apical cell surface. *Cell.* 68:533–544.

Dietrich, C., L. Bagatolli, M. Levi, Z. Volovyk, N. L. Thompson, K. Jacobson, and E. Gratton. 2001. Lipid rafts reconstituted in model membranes. *Biophys. J.* 80:1417–1428.

Draberova, L., and P. Draber. 1993. Thy-1 glycoprotein and src-like protein-tyrosine kinase p53/p5lyn are associated in large detergent-resistant complexes in rat basophilic leukemia cells. *Proc. Natl. Acad. Sci. U.S.A.* 90:3611–3615.

Heider, J. G., and R. L. Boyett. 1978. The picomole determination of free and total cholesterol in cells in culture. *J. Lipid Res.* 19:514–518.

Hoessli, D., and E. Rungger-Brandle. 1985. Association of specific cell-surface glycoproteins with a triton X-100-resistant complex of plasma membrane proteins isolated from T-lymphoma cells. *Exp. Cell Res.* 156:239–250.

Holowka, D., E. Sheets, and B. Baird. 2000. Interactions between FceRI and lipid raft components are regulated by the actin cytoskeleton. *J. Cell Sci.* 113:1009–1019.

Jacobson, K., and C. Dietrich. 1999. Looking at lipid rafts? *Trends Cell Biol.* 9:84–92.

Kusumi, A., and Y. Sako. 1996. Cell surface organization by the membrane skeleton. *Curr. Surface Org. Membr. Skel.* 8:566–74.

Kusumi, A., Y. Sako, and M. Yamamoto. 1993. Confined lateral diffusion of membrane receptors as studied by single particle tracking (nanovid microscopy): effects of calcium-induced differentiation in cultured epithelial cells. *Biophys. J.* 65:2021–2040.

Lee, G. M., A. Ishiara, and K. Jacobson. 1991. Direct observation of Brownian motion of lipids in a membrane. *Proc. Natl. Acad. Sci. U.S.A.* 88:6274–6278.

Madore, N., K. Smith, C. Graham, A. Jen, K. Brady, S. Hall, and R. Morris. 1999. Functionally different GPI proteins are organized in different domains on the neuronal surface. *EMBO J.* 18:6917–6926.

Oliferenko, S., K. Paiha, T. Harder, V. Gerke, C. Schwärzler, H. Schwarz, H. Beug, U. Günthert, and L. A. Huber. 1999. Analysis of CD44-containing lipid rafts: recruitment of annexin II and stabilization by the actin cytoskeleton. *J. Cell Biol.* 146:843–854.

Pralle, A., P. Keller, E. L. Florin, K. Simons, and J. K. Horber. 2000. Sphingolipid-cholesterol rafts diffuse as small entities in the plasma membrane of mammalian cells. *J. Cell Biol.* 148:997–1007.

Rodgers, W., and J. Zavzavadjian. 2001. Glycolipid-enriched membrane domains are assembled into membrane patches by associating with the actin cytoskeleton. *Exp. Cell Res.* 267:173–183.

Saxton, M. J., and K. Jacobson. 1997. Single-particle tracking: applications to membrane dynamics. *Annu. Rev. Biophys. Biomol. Struct.* 26: 373–399.

Schutz, G., G. Kada, V. Pastushenko, and H. Schindler. 2000. Properties of lipid microdomains in a muscle cell membrane visualized by single molecule microscopy. *EMBO J.* 19:892–901.

Sheets, E. D., G. M. Lee, R. Simson, and K. Jacobson. 1997. Tansient confinement of a glycosylphosphatidyl-anchored protein in the plasma membrane. *Biochemistry.* 36:12449–12458.

Simons, K., and E. Ikonen. 1997. Functional rafts in cell membranes. *Nature.* 387:569–572.

Simons, K., and E. Ikonen. 2000. Cell biology: how cells handle cholesterol. *Science.* 290:1721–1726.

Simson, R., E. D. Sheets, and K. Jacobson. 1995. Detection of temporary lateral confinement of membrane proteins using single tracking analysis. *Biophys. J.* 69:989–993.

Simson, R., B. Yang, S. E. Moore, P. Doherty, F. S. Walsh, and K. A. Jacobson. 1998. Structural mosaicism on the submicron scale in the plasma membrane. *Biophys. J.* 74:297–308.

Stahlhut, M., and B. v. Deurs. 2000. Identification of filamin as a novel ligand for caveolin-1: evidence for the organization of caveolin-1-associated membrane domains by the actin cytoskeleton. *Mol. Biol. Cell.* 11:325–337.

Stauffer, T., and T. Meyer. 1997. Compartmentalized IgE receptor-mediated signal transduction in living cells. *J. Cell Biol.* 139:1447–1454.

Suzuki, K., F. Sanematsu, T. Fujiwara, M. Edidin, and A. Kusumi. 2001. A GPI-anchored membrane protein, CD59, frequently visits/forms rafts in signaling: a single molecule study. *Biophys J.* 80:252a.

Tomishige, M., Y. Sako, and A. Kusami. 1998. Regulation mechanism of the lateral diffusion of band 3 in erythrocyte membranes by the membrane skeleton. *J. Cell Biol.* 142:989–1000.

Varma, R., and S. Mayor. 1998. GPI-anchored proteins are organized in submicron domains at the cell surface. *Nature.* 394:789–801.

Wu, E.-S., K. Jacobson, and D. Papahadjopoulos. 1977. Lateral diffusion in phospholipid multibilayers measured by fluorescence recovery after photobleaching. *Biochemistry.* 16:3936–3943.